Int. J. Electrochem. Sci., 15 **(2020)** 11769 – 11778, doi: 10.20964/2020.12.63

International Journal of
ELECTROCHEMICAL
SCIENCE
www.electrochemsci.org

Short Communication

Preparation of highly dispersed Ru-Ni alloy nanoparticles on an N-doped carbon layer (RuNi@CN) and its application as a catalyst for the hydrogen evolution reaction in alkaline solution

Wei Wang[1], *Jiaqian Peng*[1], *Lehao Yang*[2], *Qinglei Liu*[1,*], *Yongfei Wang*[2,3,*], *Huimin Liu*[1,*]

[1] School of perfume and aroma technology, Shanghai Institute of Technology, 100#, Haiquan Road, Shanghai 201418, PR China
[2] School of Chemical Engineering, University of Science and Technology Liaoning, 185#, Qianshan Zhong Road, Anshan 114044, PR China
[3] School of Materials and Metallurgy, University of Science and Technology Liaoning, 185#, Qianshan Zhong Road, Anshan 114044, PR China
[*]E-mail: 546072820@qq.com, wyf8307@ustl.edu.cn , szliuhm@163.com

Received: 17 August 2020 / *Accepted:* 3 October 2020 / *Published:* 31 October 2020

The hydrogen evolution reaction (HER) with transition metal alloys, as a substitute for platinum-based catalysts, under alkaline conditions is being increasingly studied. In this paper, a high dispersion of Ru-Ni alloy nanoparticles on an N-doped carbon layer (RuNi@CN) were synthesized by calcining a solid mixture of D-glucosamine hydrochloride (GAH), melamine, $RuCl_3$ and $Ni(NO_3)_2 \cdot 6H_2O$ in an inert atmosphere. The calcination temperature was an important factor that affected the electrocatalytic performance of RuNi@CN. The RuNi@CN electrocatalyst obtained under optimized conditions showed high efficiency and stable activity for the HER over a wide range of pH values, especially under alkaline conditions. The overpotentials of RuNi@CN-700 at 10 and 100 mA cm^{-2} were 76.26 and 213.69 mV, respectively, with a Tafel slope of 66.35 mV dec^{-1}. Ruthenium is the cheapest platinum group metal, and its content in the catalyst was only 0.1209 wt%. Thus, this study shows the high activity and competitive price of this prepared catalyst.

Keywords: Ru-Ni alloy; Hydrogen evolution reaction, nanoparticles; electrocatalysis

1. INTRODUCTION

With the rapid development of the social economy, the increased consumption of fossil fuels and the subsequent increase in environmental pollution are becoming more serious. Therefore, establishing a global sustainable energy system is the key to solving this problem while also protecting the environment [1-3]. Hydrogen is the most promising clean energy. The use of electrolyzed water is currently an effective way to produce hydrogen [4]. Platinum (Pt)-based materials are still the best

catalysts for hydrogen production from electrolyzed water. However, Pt has limitations in practical, large-scale H_2 production due to its high cost, scarcity and poor electrochemical stability [5,6]. Therefore, researchers are currently working on alternatives to Pt-based materials.

Nitrogen-doped carbon nanomaterials have been used in a wide range of electrocatalysis applications due to their high specific surface area, good electrical conductivity and controllable molecular structure [7-13]. The nitrogen atoms doped in the carbon matrix adjust the electronic properties of adjacent carbon atoms through intramolecular charge transfer, which is beneficial for improving the electrocatalytic performance [14]. The interaction between the supported metal core and nitrogen-doped carbon can promote electron transfer, change the charge distribution on the surface of the carbon layer to generate a sufficient number of local active sites and change the Gibbs free energy of the adsorbed reactants to promote the electrocatalytic evolution of hydrogen [15,16].

Ruthenium (Ru, $290 per oz) is a cheaper alternative to Pt ($992 per oz), being one-third of the price. Compared with Pt, Ru possesses a similar metal bond strength to hydrogen (~65 kcal mol^{-1}). According to the experimental results and DFT calculations, Ru hardly decreases the catalytic efficiency of the HER [17-19]. In addition, Ru shows good stability under both acidic and basic conditions, making this metal extremely versatile in terms of application. As a precious metal, Ru still faces problems, such as its high cost and scarcity. Therefore, the premise of ensuring its stability and high activity is to increase its atomic utilization to reduce costs. From the Brewer-Engel valence bond theory, it is known that metal elements with empty or semifilled d orbitals form alloys with metal elements that have a number of d electrons greater than the number of d orbitals (that is, pairs of d electrons), thus generating electricity for the hydrogen evolution reaction. Catalytic synergy greatly improves the electrocatalytic hydrogen evolution activity of the electrode [20]. Therefore, alloying inexpensive transition metal atoms with a small amount of precious metal (Ru), for instance producing a RuM@CN electrocatalyst, can significantly improve the catalytic performance [21]. This result indicates that a new and efficient HER catalyst can be prepared by the combination of a Ru-based alloy and a carbon material.

Herein, highly dispersed RuNi NPs over N-doped carbon hybrids (RuNi@CN) were directly synthesized through the calcination of a solid mixture of D-glucosamine hydrochloride (GAH), melamine, $RuCl_3$ and $Ni(NO_3)_2{\cdot}6H_2O$. The obtained RuNi@CN was proposed as a possible cathode for hydrogen generation in an alkaline medium, and it exhibited an electrocatalytic hydrogen evolution performance comparable to that of commercial Pt/C. The low overpotentials of the catalyst at 10 and 100 mA cm^{-2} were 76.26 and 213.69 mV, respectively. The Tafel slope was 66.35 mV dec^{-1}, the electrochemical capacitance (Cdl) was 7.84 mF/cm, and the charge transfer resistance was 79.27 Ω.

2. EXPERIMENTAL

2.1 Synthesis of RuNi@CN

First, GAH (100 mg), melamine (2 g), $RuCl_3{\cdot}3H_2O$ (10 mg) and $Ni(NO_3)2{\cdot}6H_2O$ (110 mg) were fully mixed in the proper amount of deionized water. After evaporative drying, the mixture was transferred to a high temperature tube furnace at a heating rate of 3 ℃/min and then kept at 600 ℃ for 1

h. Next, the sample was heated to X ℃ at a rate of 2 ℃/min and kept at that temperature for 1 h to obtain RuNi@CN-X (600≤X≤1000). RuNi@CN-600, RuNi@CN-700, RuNi@CN-800, and RuNi@CN-1000 were obtained according to the above method.

2.2 Characterization

The samples were characterized by scanning electron microscopy (SEM, SIGMA HD, Germany), transmission electron microscopy (TEM, JEM-2010F, JEOL, Japan), X-ray diffraction (XRD, X'Pert PRO, PANalytical B.V., Cu Kα radiation source, λ=1.5418 Å), X-ray photoelectron spectroscopy (XPS, Newcastle, U.K.), nitrogen adsorption-desorption isotherms (Quantachrome, USA) and inductively coupled plasma optical emission spectrometry (ICP-OES, IRIS Intrepid II XSP, USA).

2.3 Electrochemical measurements

Typically, 3 mg of catalyst was dispersed in a solution containing 1 mL of a 4:1 V/V water/isopropanol mixed solvent and 30 μL of a Nafion solution (5 wt%) via ultrasonication for at least 30 min in an ice bath. Then, 5 μL of the dispersion (loading ~0.0425 mg cm^{-2}) was loaded onto a glassy carbon electrode with a diameter of 3 mm, and the modified electrode was dried at room temperature.

The HER electrochemical measurements were tested using a three-electrode system on an electrochemical workstation (*Ivium Vertex. One. EIS*) with 1 M KOH, 0.5 M H_2SO_4 and 1 M PBS solutions at room temperature. Ag/AgCl and graphite rods were used as the reference and counter electrodes, respectively, and the prepared samples were directly used as working electrodes. Before each test, nitrogen (N_2) was injected into the electrolyte to remove dissolved oxygen. N_2 gas was also injected during the experiment. The scanning rate of the linear sweep voltammetry test was 5 mV s^{-1}, and the polarization curves were compensated and corrected by IR. The long-term stability was tested by cyclic voltammetry (CV) at a scanning rate of 50 mV/s^{-1}. Additionally, electrochemical impedance spectroscopy (EIS) was performed (100 kHz~0.01 Hz).

3. RESULTS AND DISCUSSION

The structural characteristics of the RuNi@CN samples and the distribution of Ru-Ni alloy particles were studied by scanning electron microscopy (SEM) and transmission electron microscopy (TEM). In the low temperature range (≤ 600° C, Fig. 1a), melamine, as a template, is thermally polymerized to form layered graphite carbonitride (g-C3N4). At the same time, GAH is condensed in the middle layer of g-C3N4 to form a carbon skeleton, so the sample shows a large number of accumulated layers [22]. The sandwich structure can effectively prevent the agglomeration of Ru-Ni NPs and Ni NPs; however, the effect is limited [23]. With an increasing pyrolysis temperature (≥700°C, Fig. 1b), carbon nitride decomposes due to its thermal instability, forming a carbon layer of slightly wrinkled nanoflakes. The nitrogen atoms produced by the decomposition of carbon nitride are partially

doped into the carbon skeleton, thus increasing the amount of nitrogen doping [24]. When the pyrolysis temperature is 800°C (Fig. 1c), a small number of carbon nanotubes are formed because the excess number of Ni atoms catalyze the crimping of the carbon layer to form carbon nanotubes.

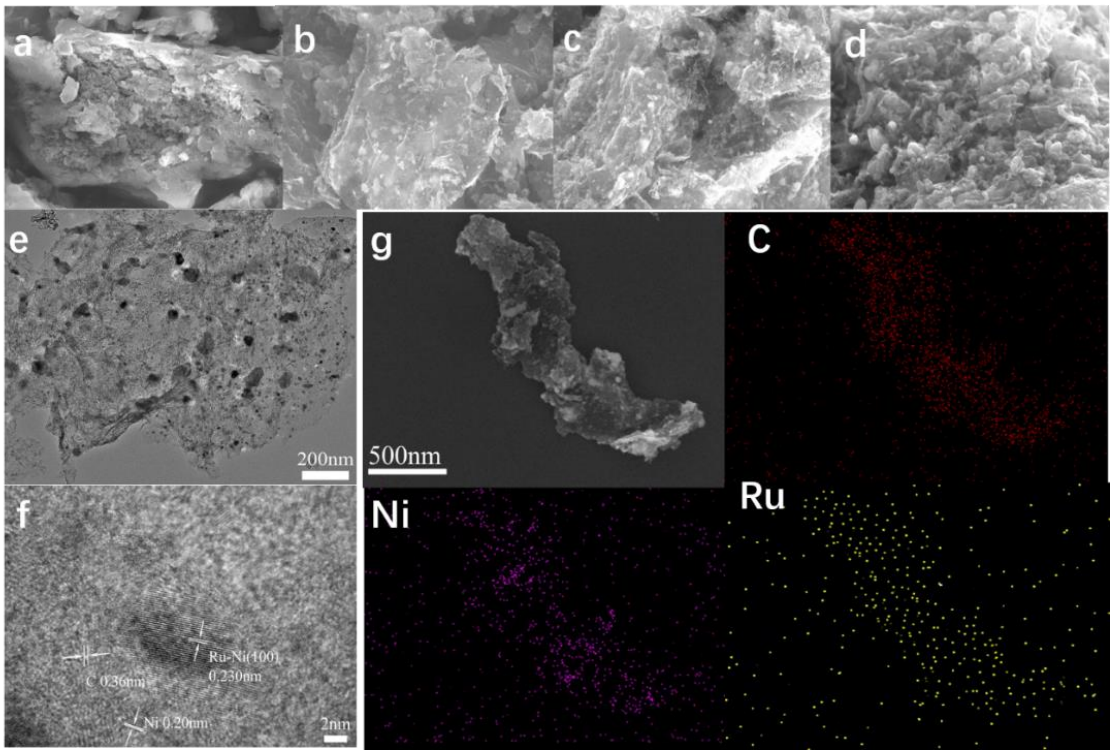

Figure 1. (a ~ d) SEM image of RuNi@CN-600, RuNi@CN-700, RuNi@CN-800, and RuNi@CN-1000; (e, f) TEM and HRTEM images of RuNi@CN-700; (g) SEM image of RuNi@CN-700 and the corresponding EDS elemental maps.

When the pyrolysis temperature is 1000°C (Fig. 1d), nickel atoms catalyze the transition of carbon layers into carbon nanotubes for their deposition. Figure 1e further reveals that RuNi@CN-700 is a layered structure composed entirely of wrinkled nanowires. From Fig. 1f, we can see the lattice stripes of the Ru-Ni alloy with a 0.230 nm plane spacing, the Ni-metal lattice stripes with a 0.200 nm plane spacing and the graphite layer with a 0.360 nm layer spacing. The Ni-Ru alloy with diameters of 10-20 nm and Ni nanoparticles are uniformly dispersed on the layered carbon materials, which may be due to the good anchoring of the sandwiched structure and the negatively charged N in the carbon material [25, 26]. Figure 1g shows that the Ni and Ru elements evenly cover the selected area on the material, which is consistent with the TEM results. The specific content of both elements can be determined by ICP-OES. The content of Ni is approximately 1.951 wt.%, and the Ru content is approximately 0.1209 wt.%.

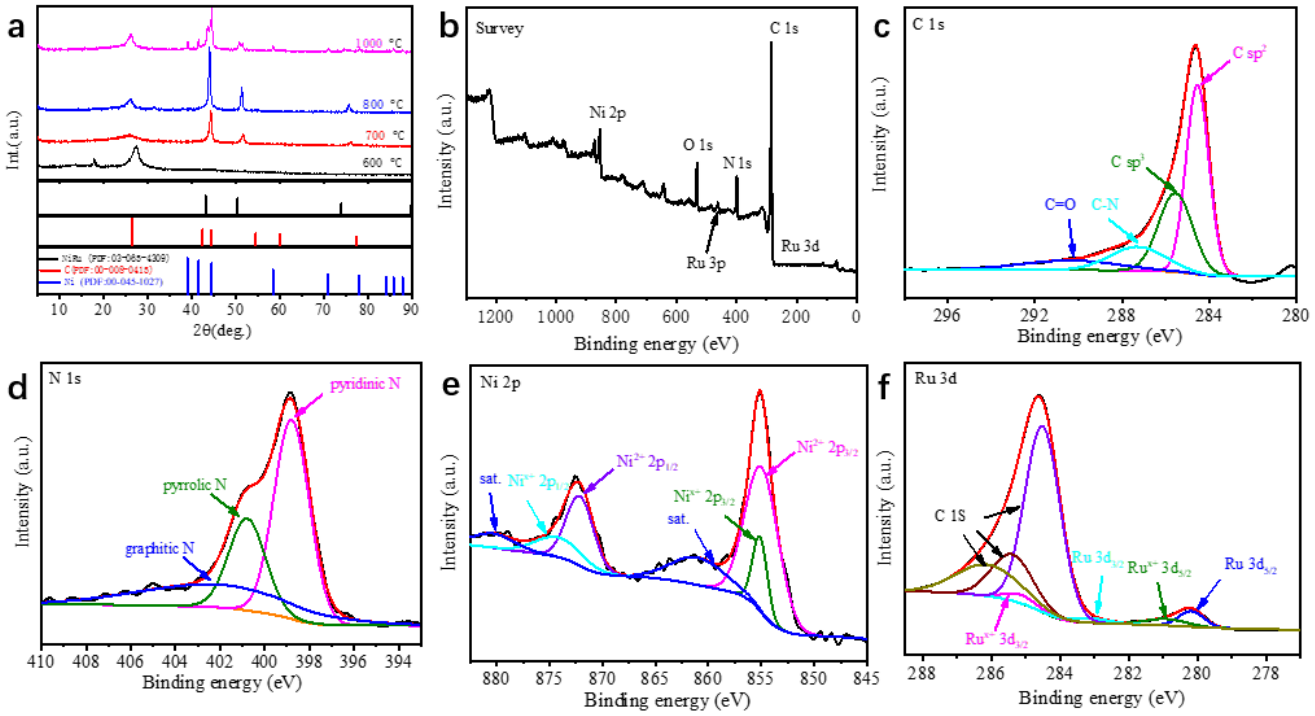

Figure 2. (a) XRD spectra of the RuNi@CN samples at different annealing temperatures; (b) XPS full spectrum of RuNi@CN-700; (c~ f) are the high-resolution spectra of C 1s, N 1s, Ni 2p, and Ru 3d of RuNi@CN-700.

Figure 2a shows that a weak and wide peak appears at 26°, which is the characteristic diffraction peak of the graphite lattice (002), indicating that an ultrathin graphitized carbon layer has been formed. The Ru-Ni alloy is dispersed on the carbon layer at peak positions of 44, 52 and 76°. The crystal structure of the Ru-Ni alloy depends on the relative content of Ru and Ni. The Ru-Ni alloy shows a face-centered cubic (fcc) structure for the most part, so the crystal structure of RuNi@CN samples is fcc [27]. In addition, there is no diffraction peak corresponding to Ru in the spectrum, indicating that Ru is alloyed with nickel.

To further analyze the elemental composition and chemical valence of RuNi@CN samples, XPS analysis was carried out on RuNi@CN-700. As shown in Fig. 2b, the sample carbonized at high temperature contains five elements: C, N, O, Ni and Ru. Figure 2c shows the high-resolution XPS spectrum of C 1s. The C 1s orbitals include a C = C bond at 284.53 eV, a C-C bond at 285.54 eV, a C-N bond at 287.27 eV and a C = O bond at 290.38 eV, in which the C = C bond and C - C bond come from the carbon skeleton of GAH. The existence of a C-N bond shows that N has been successfully doped into the carbon structure [28]. The existence of a C=O bond indicates that there are a certain number of oxygen-containing functional groups on the sample surface, which can effectively improve the hydrophilicity of the carbon material and is beneficial to the preparation of catalyst ink for improving the electrical conductivity. From Fig. 2d, three typical types of nitrogen can be observed: pyridinic nitrogen at 398.80 eV, pyrrolic nitrogen at 400.80 eV, and graphitic nitrogen at 401.63 eV, in which the pyridinic nitrogen is dominant. These results show that nitrogen atoms are successfully doped into the

carbon skeleton, which enhances the interaction between the sample and adsorbed hydrogen atoms. Figure 2e is the Ni 2p fitting XPS spectrum. It can be seen from the figure that Ni^0 and Ni^{x+} coexist in the sample. The characteristic peaks of 854.93 and 872.14 eV correspond to the $Ni2p_{3/2}$ and $Ni2p_{1/2}$ orbitals, respectively. The characteristic peaks at 855.13 and 874.12 eV are the characteristic peaks of Ni^{x+}, and the peaks at 861.01 and 880.31 eV are the characteristic satellite peaks of $Ni2p_{3/2}$ and $Ni2p_{1/2}$, respectively. Figure 2f shows the Ru 3D-fitting XPS spectrum, and it is found that Ru^0 and Ru^{x+} coexist. The characteristic peaks of $Ru^03d_{5/2}$ and $Ru^03d_{3/2}$ are at 280.17 and 283.13 eV, respectively. The characteristic peaks at 280.92 and 285.16 eV can be attributed to $Ru^{x+}3d_{5/2}$ and $Ru^{x+}3d_{3/2}$. The fitting peak at approximately 287.0 eV is the C 1s peak.

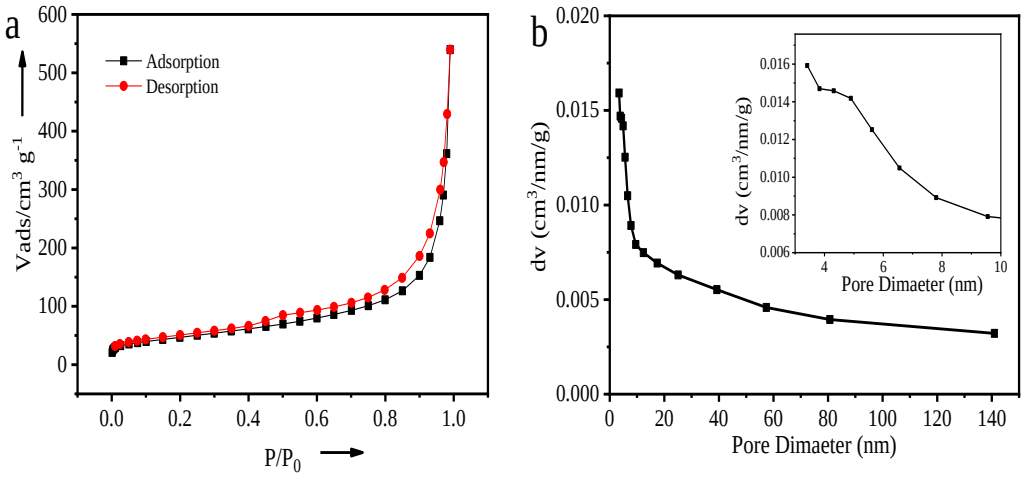

Figure 3. N_2 adsorption/desorption isotherms and the BJH pore-size distribution curves of RuNi@CN-700.

The specific surface area and channel information of the RuNi@CN-700 samples were analyzed by the N_2 adsorption-desorption method. Figure 8a shows the N_2 adsorption-desorption isotherm of the sample. The isotherm shows a typical type-IV curve. The specific surface area of the sample measured by the specific surface area method is 167.657 m^2 g^{-1}, indicating that the sample has a high specific surface area. Figure 8b shows the pore size distribution of the sample calculated by the BJH method. The sample mainly contains two types of pores: mesopores, which are predominant, and macropores. The average pore volume and pore diameter of the samples are 0.801 cm^3 g^{-1} and 3.412 nm, respectively, which are consistent with the results of the scanning electron microscopy (SEM) and transmission electron microscopy (TEM) results. The detailed analysis of the adsorption isotherm shows that when the relative pressure P/P0 < 0.1, the adsorption isotherm increases slightly, indicating that there is a small number of micropores in RuNi@CN-700, and the pore size distribution is not well reflected. A large hysteresis loop appears in the isotherm near P/P0 = 0.5, indicating that the sample has a mesoporous structure. The existence of mesopores improves the process of catalytic mass transfer. When P/P0 $\geqslant$ 0.8, the isotherm suddenly increases, which further indicates that the sample has a very porous structure. The macropores mainly come from the stacked pores between graphene layers. It can be inferred that

the sample has many lamellar structures. Therefore, the RuNi@CN-700 sample has a multistage pore structure.

Table 1. Overpotentials of the different samples

Samples	pH=0.34 η_{10} (mV vs. RHE)	pH=14 η_{10} (mV vs. RHE)	pH=7 η_{10} (mV vs. RHE)
RuNi@CN-600	-	-	-
RuNi@CN-700	96.59	76.26	143.58
RuNi@CN-800	183.84	323.64	597.37
RuNi@CN-1000	332.36	336.64	603.54
20% Pt/C	17.49	30.68	58.57

To study the catalytic performance of the samples at different pyrolysis temperatures, the results of hydrogen evolution of the samples over the whole pH range are shown in Table 1. It can be seen from Table 1 and Fig. 4a that the sample shows better hydrogen evolution performance when the pyrolysis temperature is 700°C. Especially in 1 M KOH, the overpotential of commercial Pt/C is 76.26 and 213.69 mV at 10 and 100 mA cm^{-2}, respectively. As seen from the Tafel slope diagram in Fig. 4b, the Tafel slope of RuNi@CN-700 is 66.35 mV dec^{-1} in 1 M KOH. The HER reaction follows the Volmer-Heyrovsky mechanism, and desorption (Heyrovsky reaction) is the rate-controlling step [29,30]. Fig. 4c shows that under alkaline conditions, the double layer capacitances of RuNi@CN-700, RuNi@CN-800 and RuNi@CN-1000 are 7.84, 1.61 and 1.285 mF cm^{-2}, respectively. It is known that the electric double layer capacitance of an electrocatalyst is proportional to the effective catalytic area of the catalyst. Therefore, when the pyrolysis temperature is 700°C, the effective catalytic area is larger, and there are more bare surfaces [31]. The AC impedance spectra under alkaline conditions are fitted with the equivalent circuit model shown in Fig. 4d, where Rs is the solution resistance, Rct is the charge transfer resistance, and CPE is the constant phase element [32]. The charge transfer resistance (Rct) of the RuNi@CN-700 sample is the smallest, which is close to that of Pt/C, so its charge transfer rate is the fastest. Furthermore, the Nyquist curve of RuNi@CN-700 is a semicircle with the smallest radius, and the higher the pyrolysis temperature is, the larger its Rct [33]. These results are consistent with the electrochemical catalysis performance of RuNi@CN-700. Stability is another important index to evaluate electrocatalysts. The durability of RuNi@CN-700 was studied by scanning 2000 cycles at a scanning rate of 5 mV/s^{-1}. As shown in Fig. 4e, the performance at 700 s declines slightly before and after 2000 cycles. These results show that the RuNi@CN-700 catalyst has good stability. Moreover, the HER catalytic activity of RuNi@CN-700 is close to or higher than that of other reported ruthenium catalysts (see Table 2) when measured at the same current density.

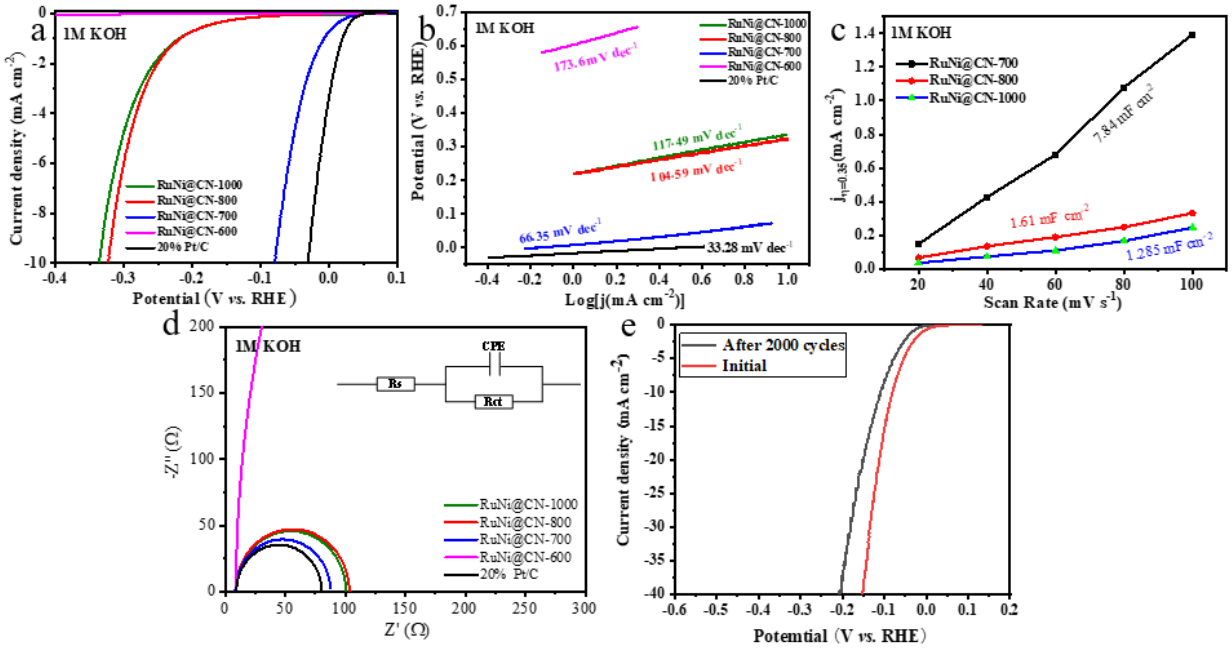

Figure 4. HER polarization curves (a) and Tafel plots (b) for the RuNi@CN samples and Pt/C catalyst. (c) Current density as a function of the scan rate for RuNi@CN samples. (d) Nyquist curves for the RuNi@CN samples and Pt/C catalyst at η=10 mV. (e) HER polarization curves of RuNi@CN-700 recorded before and after 2000 potential cycles.

Table 2. Comparison of some recently reported Ru-based and other representative HER electrocatalysts in alkaline electrolytes.

Catalyst	Overpotential at corresponding jη10 (mV vs. RHE)	Tafel slope (mV decade-1)	References
RuNi@CN	76.26	66.35	This work
Ru-CoNi@NC-2	268	63	[34]
$SrRuO_3$/CNT	109 ± 3.39	45	[35]
N, Ru codoped Sb_2S_3	72	193	[36]
Ni_3S_2 nanorods	162	106	[37]
$Pd_{83.5}Ir_{16.5}$	73	43.6	[38]
Cu_2-xS@RuNPS	82	48	[39]
Ru/CP	78	50	[40]
Porous Ru nanomaterial	83	80	[41]
$Ru/C_3N_4/C$	79	-	[42]

4. CONCLUSION

In summary, we show a simple method for preparing RuNi@CN by pyrolysis. RuNi@CN-700 is a highly efficient electrocatalyst that shows good HER activity over a wide range of pH values. Especially in alkaline solution, its catalytic activity is close to that of Pt/C. Ru is a platinum group metal, but its cost is much lower than that of Pt. Therefore, the study of these potential RuNi@CN electrocatalysts provides research value in the exploration of electrocatalysts that can replace Pt catalysts in the field of energy conversion.

ACKNOWLEDGMENTS
We gratefully acknowledge the Natural Science Foundation of Liaoning Province (No. 2019-ZD-0266).

References

1. J. A. Turner, *Science,* 305(2004) 972.
2. S. Chu, A. Majumdar, *Nature*, 488(2012) 294.
3. N. S. Lewis, D. G. Nocera, *Proc. Natl. Acad. Sci. U.S.A,* 103(2006) 15729.
4. M. S. Dresselhaus, I. L. Thomas, *Nature*, 414(2001) 332.
5. V. R. Stamenkovic, B. S. Mun, M. Arenz, *Nature Materials*, 6(2007) 241.
6. J. R. McKone, E. L. Warren, M. J. Bierman, *Energy & Environmental Science,* 4(2011) 3573.
7. M. Chhetri, S. Maitra, H. Chakraborty, *Energy & Environmental Science,* 9(2016)95.
8. J. Zhang, L. Qu, G. Shi, J. Liu, J. Chen and L. Dai, *Angew. Chem. Int. Ed.*, 55(2016) 2230.
9. Y. Ito, W. Cong, T. Fujita, Z. Tang and M. Chen, *Angew. Chem. Int. Ed.*, 54(2015) 213.
10. B. R. Sathe, X. X. Zou, T. Asefa, *Catalysis Science & Technology*, 4(2014) 2023.
11. J. J. Duan, S. Chen, M. Jaroniec, *Acs Nano*, 9(2015) 931.
12. Y. Zheng, Y. Jiao, Y. Zhu, L. H. Li, Y. Han, Y. Chen, A. Du, M. Jaroniec and S. Z. Qiao, *Nat. Commun.,* 5(2014) 3783.
13. J. Deng, M. Li, Y. Wang, *ChemInform,* 18(2016) 4824.
14. K. Gong, F. Du, Z. Xia, *Science*, 323(2009) 760.
15. J. Su, Y. Yang, G. Xia, J. Chen, P. Jiang and Q. Chen, *Nat. Commun.*, 8(2017) 14969.
16. Y. Yang, Z. Lin, S. Gao, J. Su, Z. Lun, G. Xia, J. Chen, R. Zhang and Q. Chen, *ACS Catal.*, 7(2017) 469.
17. Y. Zheng, Y. Jiao, Y. Zhu, L. H. Li, Y. Han, Y. Chen, M. Jaroniec and S.-Z. Qiao, *J. Am. Chem. Soc.*, 138(2016) 16174.
18. R. K. Shervedani and A. Amini, *Carbon*, 93(2015) 762.
19. J. Mahmood, F. Li, S.-M. Jung, M. S. Okyay, I. Ahmad, S.-J. Kim, N. Park, H. Y. Jeong and J.-B. Baek, *Nat. Nanotech.*, 12(2017) 441.
20. M. M. Jaksic, Electrochimica *Acta* 29(1984) 1539.
21. J. Su, Y. Yang, G. Xia, *Nature Communications*, 8(2017) 14969.
22. Y. Wang, X. C. Wang and M. Antonietti, *Angew. Chem. Int. Ed.*, 51(2012) 68.
23. X.-H. Li, S. Kurasch, U. Kaiser and M. Antonietti, *Angew. Chem. Int. Ed.*, 51(2012) 9689.
24. J. Wang, Z. Wei, Y. Gong, S. Wang, D. Su, C. Han, H. Li and Y. Wang, *Chem. Commun.*, 51(2015) 12859.
25. M. Tang, S. Mao, M. Li, Z. Wei, F. Xu, H. Li and Y. Wang, *ACS Catal.*, 5(2015) 3100.
26. J. Ding, Q. Shao, Y. Feng, *Nano Energy*, 47(2018) 1.
27. R. Dhanda, M. Kidwai, *ChemistrySelect*, 2(2017) 335.
28. J. Liang, Y. Jiao, M. Jaroniec and S. Z. Qiao, *Angew. Chem. Int. Ed.*, 51(2012) 11496.

29. Y. Li, H. Wang, L. Xie, *J. Am. Chem. Soc.,* 133(2011) 7296.
30. Q. L. Liu, L. H. Yang, P. Sun, H. G. Liu, J. H. Zhao, X. K. Ma, Y. F. Wang and Z. Q. Zhang, *RSC Adv*., 10(2020) 22297.
31. M. A. Lukowski, A. S. Daniel, F. Meng, A. Forticaux, L. S. Li and S. Jin, *J. Am. Chem. Soc.*, 135(2013) 10274.
32. R.D.Armstrong, M.Henderson, *Journal of Electroanalytical Chemistry and Interfacial Electrochemistry*, 39(1972) 81.
33. L. Zhu, Q. Cai, F. Liao, M. Sheng, B. Wu and M. Shao, *Electrochem. Commun.*, 52(2015) 29.
34. W. Q. Wang, S. M. Xi, Y. L. Shao, W. H. Sun, S. K. Wang, J. F. Gao, C. M. Mao, X. S. Guo, G. C. Li, ACS Sustainable Chem. Eng.,20 (2019)17227.
35. Y. K. Sugawara, K. G. Kamata, and T. Yamaguchi, *ACS Applied Energy Materials,* 2 (2019) 956.
36. A. Maiti and S. K. Srivastava, *ACS Applied Materials & Interfaces*, 12 (2020) 7057.
37. J. Y. Chen, Y. H. Ling, Z. X. Lu, and Z. J. Zhang, *ACS Applied Energy Materials*, 3 (2020) 5745.
38. C. Wang, H. Xu, H. Y. Shang, L. J. Jin, C. Y. Chen, Y. Wang, M. Y. Yuan, and Y. K. Du, *Inorganic Chemistry*, 59 (2020) 3321.
39. D. Yoon, J. Lee, B. Seo, B. Kim, H. Baik, S. H. Joo and K. Lee, *Small*, 13(2017)1700052.
40. J. L. Liu, Y. Zheng, D. D. Zhu, A. Vasileff, T. Ling and S. Z. Qiao , Nanoscale*,* 9(2017) 16616.
41. S. Drouet, J. Creus, V. Collière, C. Amiens, J. García-Antón, X. Sala and K. Philippot , *Chem. Commun.,* 53(2017) 11713.
42. Y. Zheng, Y. Jiao, Y. Zhu, L. H. Li, Y. Han, Y. Chen, M. Jaroniec, S. Z. Qiao, *J. Am. Chem. Soc.*, 138(2016) 16174.